Computational Electrochemistry: The Simulation of Voltammetry under Hydrodynamic Modulation Control

Kerry A. Gooch and Adrian C. Fisher*

Department of Chemistry, University of Bath, Claverton Down, Bath BA2 7AY, United Kingdom

Received: March 1, 2002; In Final Form: July 29, 2002

A conceptually simple and numerically efficient approach to the simulation of current/time transients under hydrodynamically modulated conditions is presented. The generality of the method is illustrated by reference to the case of hydrodynamic modulated voltammetry (HMV) within a channel cell device under pressure driven flow control. For the preliminary studies reported here, modulation refers to a stepped change in the pressure between two limits. This change occurs either instantaneously or linearly over a normalized time. The voltammetric response of a simple redox reaction is used to illustrate the predicted influence of the modulation rate on the current flowing within the flow cell. A normalization procedure is proposed to simplify data presentation and shown to be valid for a wide range of experimentally viable conditions. The simulations are also employed to assess how the current response is influenced by the form of the pressure change between two limits. Simulations are presented for cases where an instantaneous pressure change is employed and compared to results where a linear variation in the pressure is used.

Introduction

Hydrodynamic techniques have been widely exploited in the field of electrochemistry for analytical analysis, mechanistic and kinetic interpretation.[1−6] Alongside experimental developments numerical simulations have been used to permit the quantitative analysis of the experimental data.[7] In the majority of studies presented, the hydrodynamic component has been used under steady-state conditions, thus permitting analytical approximation of the velocity profile within the electrochemical cell. However, an alternative experimental strategy based on hydrodynamic modulation has also been reported within the literature. In these techniques hydrodynamic modulation voltammetry (HMV)[8−10] exploits a periodic oscillation of the mass transport rate to the electrode surface. This is achieved by either varying the solution flow rate over a stationary electrode or by moving the electrode with respect to the solution. The merits of HMV using either macro- or microelectrodes have been widely established[11−14] and include improvements in both the concentration detection limits and the stability of the electrode response.

Early experiments focused mainly on the use of tubular and channel flow cells,[15−17] through which solution was pulsed between a maximum and minimum value. These techniques have been further developed to encompass a variety of cell configurations and experimental approaches[18,19] which includes the modulated rotating disk electrode (RDE) pioneered by Bruckenstein.[20−22] However, unlike measurements reported under steady state flow conditions where numerical analysis is now routinely exploited, in the cases reported to date, quantitative analysis using HMV has been restricted to the development of semiempirical or approximate analytical solutions. In this article, we outline the development of numerical simulations which permit the inclusion of non-steady-state convective transport within channel electrode flow cells.

We have previously demonstrated[23−26] that the finite element method (FEM) is a valuable approach to the simulation of current/voltage and flow rate relationships within a variety of electrochemical devices including the channel flow cell.[7] In this article, we outline the development of this strategy to permit the time dependent variation of solution velocity. In particular, we examine the influence of hydrodynamic modulation on the current/voltage response for a range of experimentally viable conditions. Initial simulations exploit an instantaneous pressure change to alter the transport rate through the cell and results are presented which propose a normalization strategy for experimentalists working within the area.

In experimental arrangements, it is unlikely that a totally instantaneous pressure change can be achieved and a series of results are also presented where the movement between the maximum and minimum transport rates is achieved via a linear pressure change. Results are presented to highlight the influence of this behavior in comparison to the idealized instantaneous pressure jump. The approach outlined is found to be an efficient and accurate method for the simulation of voltammetric behavior under hydrodynamic modulation conditions.

Theory

We consider the current/time transients resulting from the modulation of the solution velocity through a rectangular duct, (Figure 1), corresponding to the mass transport limited reduction or oxidation of a single solution phase species A

$$A + e^- \rightleftharpoons B$$

The convective-diffusion equation describing the distribution of *A* in space (*x*,*z*) and time (*t*) can be predicted

$$\frac{\partial C_A}{\partial t} = D\frac{\partial^2 C_A}{\partial x^2} + D\frac{\partial^2 C_A}{\partial z^2} - u\frac{\partial C_A}{\partial x} - w\frac{\partial C_A}{\partial z} \qquad (1)$$

where, C_A is the concentration of species A, D is the diffusion coefficient, u and w are the velocity components and x and z are the coordinates of a point, as defined in Figure 1. We assume that sufficient electrolyte is present so that migratory transport

* To whom correspondence should be addressed. Fax: 44−1225−386231. E-mail: chsacf@bath.ac.uk.

10.1021/jp020603s CCC: $22.00
Published on Web 09/21/2002

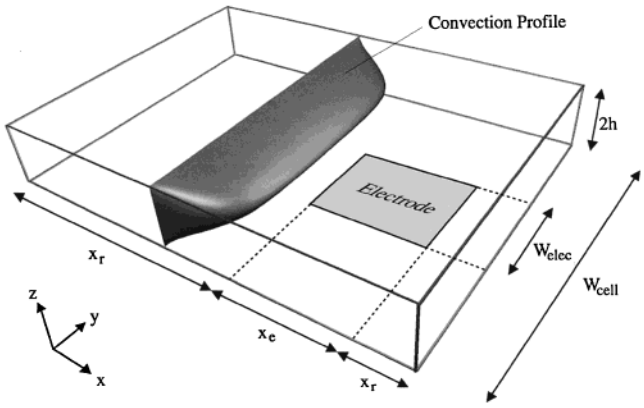

Figure 1. Channel flow cell schematic.

may be neglected. The time dependent velocities u and w may be predicted by solution of the appropriate form of the Navier−Stokes equations

$$\frac{\partial u}{\partial t} = \frac{\mu}{\rho}\left(\frac{\partial^2 u}{\partial x^2} + \frac{\partial^2 u}{\partial z^2}\right) - \frac{1}{\rho}\frac{\partial p}{\partial x} - u\frac{\partial u}{\partial x} - w\frac{\partial u}{\partial z} \quad (2)$$

$$\frac{\partial w}{\partial t} = \frac{\mu}{\rho}\left(\frac{\partial^2 w}{\partial x^2} + \frac{\partial^2 w}{\partial^2}\right) - \frac{1}{\rho}\frac{\partial p}{\partial z} - u\frac{\partial w}{\partial x} - w\frac{\partial w}{\partial z} \quad (3)$$

$$\frac{\partial u}{\partial x} + \frac{\partial w}{\partial z} = 0 \quad (4)$$

where, p is the pressure, μ is the viscosity and ρ is the density. Solution of (2−4) subject to suitable boundary conditions was performed using the finite element method, which has been used previously for the simulation of steady-state hydrodynamic properties in electrochemical devices.[7,23,24]

The Galerkin finite element method,[27,28] was selected as the approach of choice and was combined with a numerical integration method to determine the numerical contribution from each node and the Gauss−Legendre integration method leads to a high degree of accuracy.[29] Equations 2−4 were cast into matrix form using an analogous approach to that reported previously,[24] with the addition of a time dependent component $[K_T]$

$$\left([K] + \frac{2}{\partial t}[K_T]\right)\vec{U}_1 = \left(-[K] + \frac{2}{\partial t}[K_T]\right)\vec{U}_0 - [K_p](P_1 + P_0) \quad (5)$$

$$\left([K] + \frac{2}{\partial t}[K_T]\right)\vec{W}_1 = \left(-[K] + \frac{2}{\partial t}[K_T]\right)\vec{W}_0 - [K_p](P_1 + P_0) \quad (6)$$

$$[K_{ConU}]\vec{U}_1 + [K_{ConW}]\vec{W}_1 = -[K_{ConU}]\vec{U}_0 - [K_{ConW}]\vec{W}_0 \quad (7)$$

where $[K_{ConU}]$ and $[K_{ConW}]$ are the matrixes arising from the continuity equation, $[K]$ is the characteristic matrix, arising from the 2nd and 1st order terms and the pressure terms in the Navier−Stokes equations and $[K_p]$ is the load matrix, made up of the known terms and boundary conditions for the problem. The finite element formulation of the Navier−Stokes equations has been fully explored previously in the literature.[30,31] Equation 1 was cast into matrix form using an identical procedure to that reported previously[23]

$$\left([K_{CD}] + \frac{2}{\partial t}[K_{Time}]\right)\vec{C}_1 = \left(-[K_{CD}] + \frac{2}{\partial t}[K_{Time}]\right)\vec{C}_0 \quad (8)$$

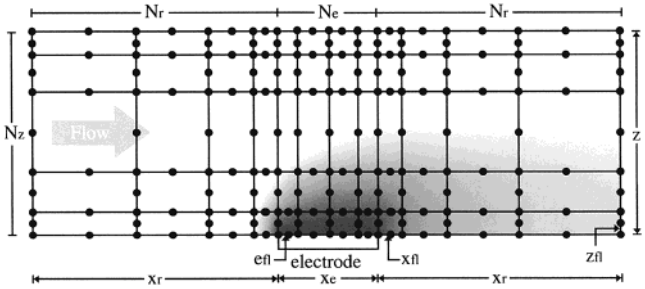

Figure 2. Grid used for two-dimensional convective-diffusion simulations with a concentration profile shown for illustration.

where $[K_{CD}]$ is the matrix made up of the convective-diffusion terms and $[K_{Time}]$ is the matrix made up of the time-dependent terms.

The problem defined by eqs (5−8) was solved by the use of a two-dimensional finite element mesh using eight noded isoparametric elements, as shown in Figure 2 where the prefix N relates to the number of elements in each direction, and the prefix X or Z relates to the cell dimensions. An f subscript in any of the labels relates to the size of the first element in that section, together with the total number of elements across the section and the total section length; define a geometric series that determines the size of the other elements.

The simulation proceeded as follows, first a fluid dynamic calculation was performed subject to the following boundary conditions, where t^* is the time when the pressure is changed and t^∞ is the end of the run.

$t^* > t \geq 0$			$t^\infty > t \geq t^*$		
$Z = 0$	all$X$	$u = 0$ $w = 0$	$Z = 0$	all$X$	$u = 0$ $w = 0$
$Z = 2h$	all$X$	$u = 0$ $w = 0$	$Z = 2h$	all$X$	$u = 0$ $w = 0$
all Z	$X = 0$	$p = 1^{st}$ set pressure	all Z	$X = 0$	$p = 2^{nd}$ set pressure
all Z	$X = 2X_r + X_e$	$p = 0$	all Z	$X = 2X_r + X_e$	$p = 0$

The calculated values of u and w were then used for the solution of eq 8 subject to the following boundary conditions:

$t = 0$			$t > 0$		
$Z = 0$	all$X$	$dC/dz = 0$	$Z = 0$	$X < X_r$	$dC/dz = 0$
$Z = 2h$	all X	$dC/dz = 0$	$Z = 0$	$X_r < X < X_r + X_e$	$C = 0$
all Z	$X = 0$	$C = C_{Bulk}$	$Z = 0$	$X_r + X_e < X$	$dC/dz = 0$
all Z	$X = 2X_r + X_e$	$dC/dx = 0$	$Z = 2h$	all X	$dC/dz = 0$
			all Z	$X = 0$	$C = C_{Bulk}$
			all Z	$X = 2X_r + X_e$	$dC/dx = 0$

yielding the concentration distribution of A at each mesh point at a specific point in time. Once complete the calculation proceeds to the next time interval and is repeated.

Current Calculation

The simulation gives the concentration distribution of species A throughout the cell as a function of time. From this the mass transport limited current (I_{Lim}) due to the oxidation/reduction of A may be calculated using

$$I_{Lim} = FDC_{Bulk}W_{elec}\sum_{i=1}^{ne}\frac{\partial x_i}{\partial z_i}\sum_{j=1}^{2}\frac{1}{2}C_{AE(i,j)} \quad (9)$$

where W_{elec} is the electrode width, F is Faraday's constant, $E(i,j)$ is an array covering each of the elements over the electrode

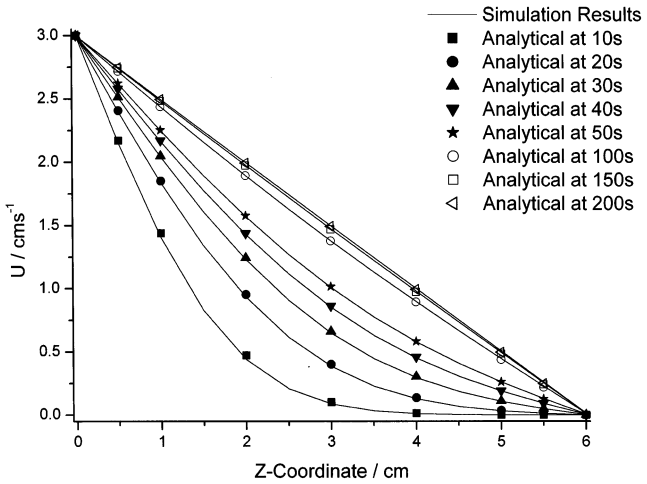

Figure 3. Transient development of couette flow between parallel plates.

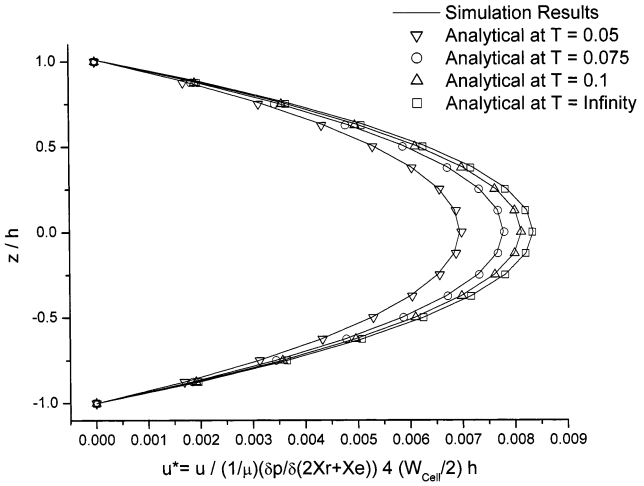

Figure 4. Transient velocity distribution for flow under a constant pressure gradient.

surface from 1 to *ne* and the two node points at the corners, and ∂x_i and ∂z_i are the dimensions of these elements.

The simulation codes were all written in Fortran 90 and run on an Intel Pentium III 600 MHz PC with 1 GB RAM. Typical run times were 90−120 min for the coupled hydrodynamic and concentration distribution codes.

Results and Discussion

Initial simulations were performed to test the validity and accuracy of the fluid dynamic calculations. Analytical solutions for the evolution of the solution velocity profile following the sudden acceleration of one wall of a rectangular duct have been reported previously[32] and numerical simulations were performed under conditions where these approximate solutions are valid. The initial boundary condition was set so that no solution flow was induced within the cell, at a specified time (t^*), the wall was moved with an applied velocity of 3.0 cms^{-1}. The velocity profile was observed to evolve (Figure 3) from the stagnant case to the steady-state linear function anticipated[31] for developing couette flow between parallel plates. The following solution properties: viscosity of 0.1 $gcm^{-1}s^{-1}$ and density of 1.0 gcm^{-3} and cell geometry: length 1 cm and height 6 cm, were used for the simulation, with a regular grid of 1 element in the *x*-direction and 6 in the *z*-direction and a time step of 1s. Figure 3 reveals both the simulated and analytically predicted response for this configuration at time steps of 10, 20, 30, 40, 50, 100, 150, and 200s and excellent agreement is observed at each time interval. Calculations were repeated for a range of different cell configurations and wall velocities and in all cases good agreement was noted.

Following the validation of the fluid dynamics aspect of the code, the boundary conditions were changed so that the top wall became stationary and the flow profile was induced by a pressure gradient across the cell. It is assumed that the simulation region being considered is after the so-called inlet region and in the Poiseuille flow region. At $t = 0$, a pressure gradient was applied (5000 $gcm^{-1}s^{-2}$ at the start of the simulation region, decreasing to 0 $gcm^{-1}s^{-2}$ at the end of the region), and allowed to reach a steady profile. Although the pressure instantaneously takes on the new value, the flow profile takes a short time to evolve to the steady values across the cell. Figure 4 shows the transient velocity distributions for a few times after the application of a pressure gradient. All values are in dimensionless form ($T = (\mu/\rho)t/W_{Cell}h$) and show good agreement with analytical theory at each time.[33] For this and all subsequent runs, the cell was 2 cm in length and 0.04 cm high and was simulated with a regular grid of 20 elements in the *x*-direction and 8 in the *z*-direction, and the time step was 0.0005 s.

TABLE 1: Pressure Range Used

first pressure ($gcm^{-1}s^{-2}$)	second pressure ($gcm^{-1}s^{-2}$)	first pressure ($gcm^{-1}s^{-2}$)	second pressure ($gcm^{-1}s^{-2}$)
10 000	5 000	2500	5000
10 000	2000	2500	1000
10 000	1000	2000	10 000
7500	5000	2000	5000
5000	10 000	2000	3000
5000	7500	2000	1000
5000	2500	1000	10 000
5000	2000	1000	5000
5000	1000	1000	2500
3000	2000	1000	2000

Next, simulations were performed to evaluate the coupled hydrodynamic and concentration distribution codes. A series of different instantaneous pressure steps were induced and the transport limited current measured once the current had established its steady-state value. The pressure steps shown in Table 1 were used for the geometry noted above and used a solution concentration of 1×10^{-3} mol dm^{-3} and a diffusion coefficient of 1×10^{-5} cm^2s^{-1}. The concentration distribution code used the following grid parameters: $Ne = 20$, $Nr = 18$, $Nz = 24$, $Xe = 0.4$ cm, $Xr = 0.8$ cm, $Z = 2h = 0.04$ cm, $efl = xfl = 5.0 \times 10^{-4}$ cm, $zfl = 5.0 \times 10^{-5}$ cm, $W_{elec} = 0.02$ cm, and $W_{cell} = 0.6$ cm. The variation of the steady-state current after the pressure step as a function of volume flow rate is shown in Figure 5. The results obtained were in good agreement with those predicted by the Levich equation for large channel based electrodes

$$I_{Lev} = 0.925nFC_{Bulk}W_{elec}x_e^{2/3}D^{2/3}\left(\frac{Vfr}{h^2W_{Cell}}\right)^{1/3} \qquad (10)$$

where Vfr is the volume flow rate ($4u_0hW_{elec}/3$), u_0 is the central velocity ($(z^2/8\mu)(\partial p/\partial(2Xr + Xe))$), and h is the half-height of the cell.

Having tested the validity of the codes, calculations were then performed to examine the voltammetric response under hydrodynamically modulated conditions.

First at a fixed volume flow rate, a potential step experiment was performed, with the potential stepped from a value insufficient to oxidize/reduce *A* to a value corresponding to the

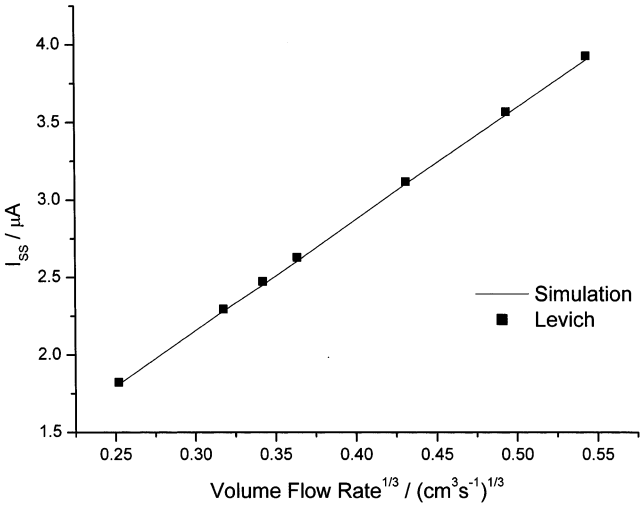

Figure 5. Simulated steady-state current after a pressure drop compares well against the Levich Prediction for a channel flow cell.

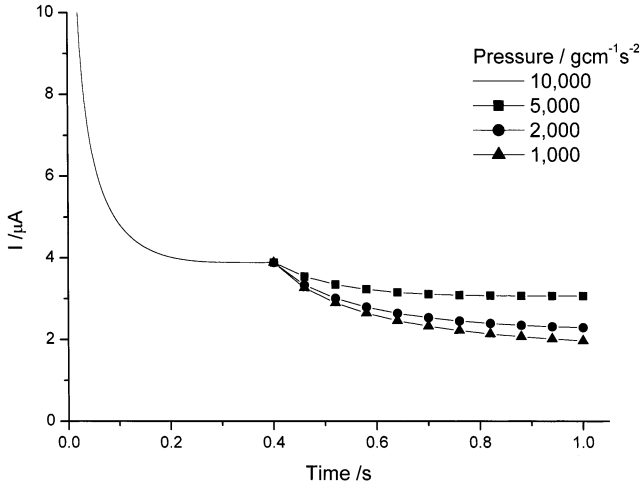

Figure 6. Current/Time Graph, showing the effect of a pressure step, for three runs all starting at a pressure of 10 000 gcm^{-1}s^{-2} (U_0 = 10 cms^{-1}) and moving to 5000, 2000, or 1000 gcm^{-1}s^{-2} at 0.4 s.

transport limited conversion to *B*. Once the steady state current had been established the applied pressure was stepped instantly to a new value and the transient current response monitored. The calculations were carried out using identical conditions to those noted above and the results presented in normalized form as noted previously,[34] using the normalized time parameter t'

$$t' = t\left(\frac{4Du_0^2}{h^2x_e^2}\right)^{1/3} \qquad (11)$$

Figure 6 shows a set of data for pressure changes from 10 000 gcm^{-1}s^{-2} to three other pressures (5000, 2000, and 1000 gcm^{-1}s^{-2}) which reveal that after the pressure step, the current undergoes an initial rapid variation before establishing a new steady-state value. It is apparent from Figure 7 that before the pressure step each current transient lies on the single normalized curve as predicted[34] for all flow rates employed. To make the normalization procedure easier, it is assumed that once the first pressure run has reached its end-point (t*), the time parameter, t, resets to zero. The normalized current (I/I_{Lim}) was obtained by dividing the current at all times by the steady-state value established at either t^* for the first pressure, or t^∞ for the second pressure. Irrespective of the initial pressure and the absolute pressure differences used, within the range indicated in Table 1, the normalized response (Figure 8 & 9) based on the ratio of initial and final pressures was found to occur.

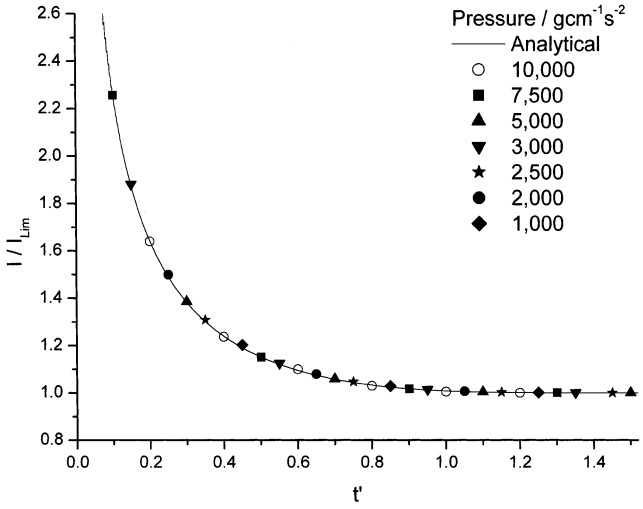

Figure 7. Current transients for each initial pressure, once normalized with respect to the central velocity and cell geometry, sit on one predicted curve.[34]

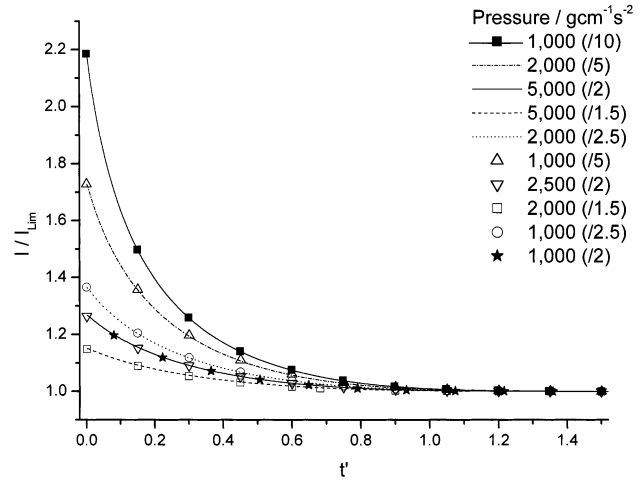

Figure 8. Current transients after a pressure decrease, once normalized form a family of curves. The symbol and number in brackets indicates the relationship between the first and second pressure.

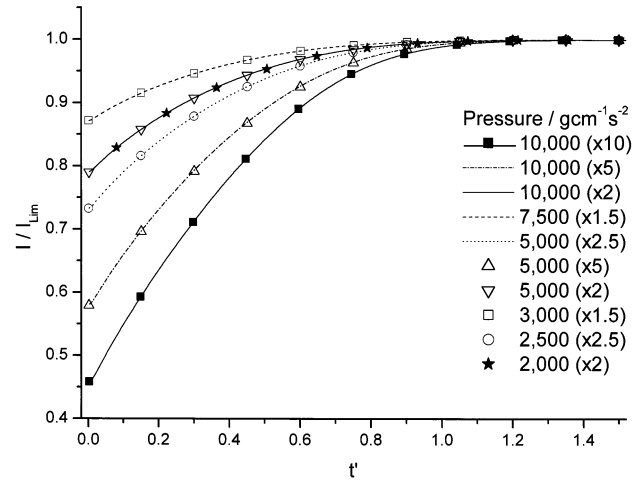

Figure 9. Current transients after a pressure increase, once normalized form a family of curves. The symbol and number in brackets indicates the relationship between the first and second pressure.

Having established a procedure for the normalization of data under conditions where an instantaneous pressure change has

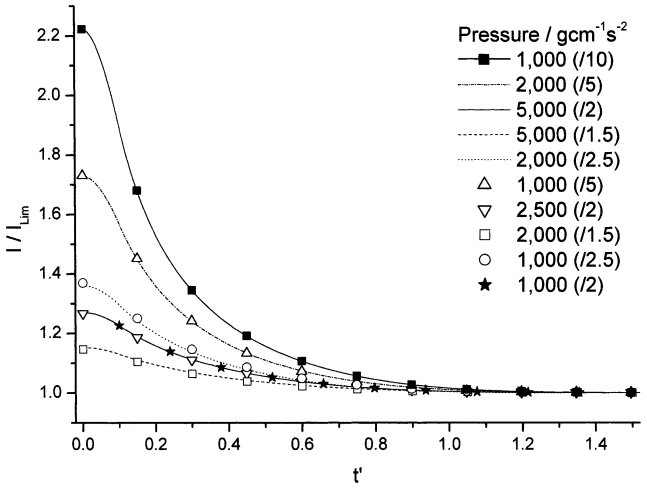

Figure 10. Current transients after a pressure decrease, once normalized form a family of curves. The new pressure is reached in a normalized time of 0.1 after the pressure change is started. The symbol and number in brackets indicates the relationship between the first and second pressure.

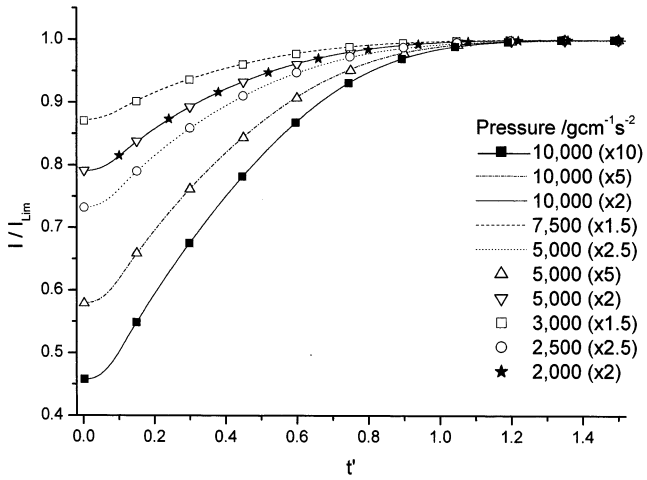

Figure 11. Current transients after a pressure increase, once normalized form a family of curves. The new pressure is reached in a normalized time of 0.1 after the pressure change is started. The symbol and number in brackets indicates the relationship between the first and second pressure.

been employed, simulations were then carried out to evaluate the effect of pressure changes that occur over a defined period of time. This condition more closely mimics experimental procedures where typically a mechanical device is used and some delay is inevitable due to the physical response time.

A linear variation in the applied pressure was chosen to illustrate the effect and for the case selected, the variation between the initial pressure and the final pressure was set to occur over the normalized time interval of 0.1. The simulation procedure was identical to that noted for the instantaneous pressure steps included above and Figures 10 and 11 reveal the normalized variation of current with time. Similar relationships to those observed in Figures 8 and 9 are again apparent; however, the approach of the current toward the steady state condition is altered significantly at short times. This is clearly due to the inability of the flow rate to reach its new value until the pressure change has been completed. This is more clearly illustrated in Figures 12 and 13, which show the difference between an instant pressure change and three linear changes (pressure variation occurs over the normalized time interval of

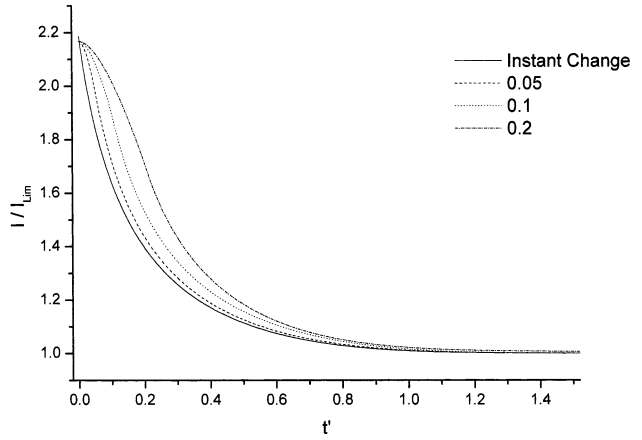

Figure 12. Comparison of instant and three linear pressure changes where the final pressure is one tenth of the initial pressure (e.g., pressure change of 10 000−1000 $gcm^{-1}s^{-2}$).

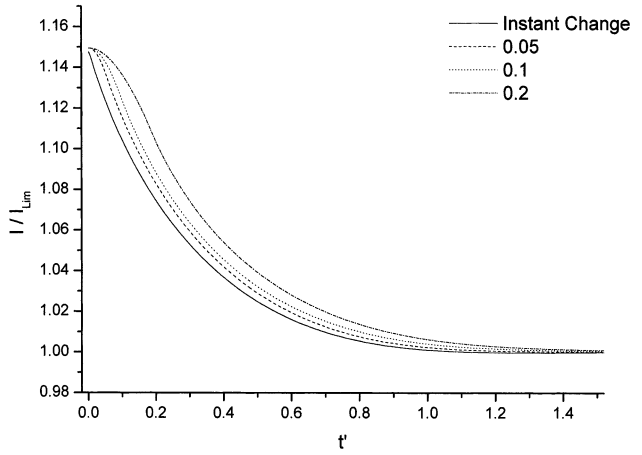

Figure 13. Comparison of instant and three linear pressure changes where the final pressure is two-thirds of the initial pressure (e.g., pressure change of 3000−2000 $gcm^{-1}s^{-2}$).

0.05, 0.1 and 0.2) for runs in which the final pressures are one tenth and two-thirds of the initial pressure, respectively.

The above results illustrate the finite element method as a flexible, easy to implement and efficient numerical strategy for the solution of voltammetric behavior under hydrodynamically modulated conditions. In addition, to the ability to quantify experimental measurements using the data presented, the above observations may assist experimental workers in assessing the efficiency of the mechanical methods used for flow modulation in flow cell devices. The extension of the above methods to examine alternative cell designs, the influence of different procedures for pressure variation (e.g., sinusoidal) and coupled kinetic complications are all currently under investigation.

Conclusion

The finite element method has been shown to be an efficient and simple procedure to assess the current/time relationships occurring under hydrodynamic modulation control. Results have been presented to assess the proposed approach, along with a normalization strategy to assist in experimental analysis of HMV data. Simulations have been performed to assess the influence of instantaneous and linear pressure variations between maximum and minimum values.

Acknowledgment. We thank the EPSRC for studentship 993 00 27X for K.A.G. and we thank Iain Henley for his help with Figures 1 and 2.

References and Notes

(1) Goldfarb, D. L.; Corti, H. R.; Marken, F.; Compton, R. G. *J. Phys. Chem. A* **1998**, *102*, 8888−8893.
(2) Unwin, P. R.; Compton, R. G. *Compr. Chem. Kinet.* **1989**, *29*, 193.
(3) Engblom, S. O.; Myland, J. C.; Oldham, K. B. *Anal. Chem.* **1994**, *66*, 3182−3187.
(4) Alden, J. A.; Compton, R. G.; Dryfe, R. A. W. *J. Electroanal. Chem.* **1995**, *397*, 11−17.
(5) Alden, J. A.; Compton, R. G. *J. Phys. Chem. B* **1997**, *101*, 8941−8954.
(6) Aixill, W. J.; Alden, J. A.; Prieto, F.; Waller, G. A.; Compton, R. G.; Rueda, M. *J. Phys. Chem. B* **1998**, *102*, 1515−1521.
(7) Stevens, N. P. C.; Fisher, A. C. *J. Phys. Chem. B* **1997**, *101*, 8259−8263.
(8) Wang, J. *Talanta* **1981**, *28*, 369−376.
(9) Deslouis, C.; Tribollet, B. *Adv. Electrochem. Sci. Eng.* **1991**, *2*, 205.
(10) Williams, D. E.; Macpherson, J. M. *Compr. Chem. Kinet.* **1999**, *37*, 369−438.
(11) Blaedel, W. J.; Olsen, C. L.; Sharma, L. R. *Anal. Chem.* **1963**, *35*, 2100.
(12) Blaedel, W. J.; Klatt, L. N. *Anal. Chem.* **1966**, *38*, 879−883.
(13) Compton, R. G.; Sealy, G. R. *J. Electroanal. Chem.* **1983**, *145*, 35−41.
(14) Moldoveanu, S.; Anderson, J. L. *J. Electroanal. Chem.* **1984**, *175*, 67−77.
(15) Blaedel, W. J.; Boyer, S. L. *Anal. Chem.* **1971**, *43*, 1538−1540.
(16) Blaedel, W. J.; Wang, J. *Anal. Chem.* **1979**, *51*, 799−802.
(17) Blaedel, W. J.; Iverson, D. G. *Anal. Chem.* **1977**, *49*, 1563−1566.
(18) Tribollet, B.; Newman, J. *J. Electrochem. Soc.* **1983**, *130*, 2016−2026.
(19) Rosamilia, J. M.; Miller, B. *Anal. Chem.* **1983**, *55*, 1142−1145.
(20) Miller, B.; Bruckenstein, S. *Anal. Chem.* **1974**, *46*, 2026−2033.
(21) Tokuda, K.; Bruckenstein, S.; Miller, B. *J. Electrochem. Soc.* **1975**, *122*, 1316−1322.
(22) Tokuda, K.; Bruckenstein, S. *J. Electrochem. Soc.* **1979**, *126*, 431−436.
(23) Fulian, Q.; Stevens, N. P. C.; Fisher, A. C. *J. Phys. Chem. B* **1998**, *102*, 3779−3783.
(24) Stevens, N. P. C.; Gooch, K. A.; Fisher, A. C. *J. Phys. Chem. B* **2000**, *104*, 1241−1248.
(25) Stevens, N. P. C.; Fulian, Q.; Gooch, K. A.; Fisher, A. C. *J. Phys. Chem. B* **2000**, *104*, 7110−7114.
(26) Qiu, F. L.; Gooch, K. A.; Fisher, A. C.; Stevens, N. P. C.; Compton, R. G. *Anal. Chem.* **2000**, *72*, 3480−3485.
(27) Rao, S. S. *The Finite Element Method in Engineering*; Pergamon Press: Oxford, 1982.
(28) Zienkiewicz, O. C.; Taylor, R. L. *The Finite Element Method*, 5th ed.; Butterworth-Heinemann: Oxford, 2000.
(29) Taylor, C.; Hughes, T. G. *Finite Element Programming of the Navier−Stokes Equations*; Pineridge Press: Swansea, 1981.
(30) Curvelier, C.; Segal, A.; van Steenhoven, A. A. *Finite Element Methods and Navier−Stokes Equations;* D. Reidel Publishing Company: Dordrecht, Holland, 1986.
(31) Taylor, C.; Hood, P. *Comput. & Fluids* **1973**, *1*, 73−100.
(32) Schlichting, H. *Boundary Layer Theory*, 7th ed.; McGraw-Hill: London, 1987.
(33) Fan, C.; Chao, B.-T. *ZAMP* **1965**, *16*, 351−360.
(34) Aoki, K.; Tokuda, K.; Matsuda, H. *J. Electroanal. Chem.* **1986**, *209*, 247−258.